

Surface wave focusing effects: Numerical modeling and statistical observations

B.G. Bukchin^{a,b}, T.B. Yanovskaya^c, J.-P. Montagner^{b,*},
A.Z. Mostinskiy^{a,b}, E. Beucler^d

^a *International Institute for Earthquake Prediction Theory and Mathematical Geophysics, Moscow, Russian Federation*

^b *Département de Sismologie, UMR 7580, Institut de Physique du Globe de Paris, France*

^c *Institute of Physics, St-Petersburg University, Petrodvoretz, St.Petersburg, Russian Federation*

^d *Laboratoire de Planétologie et Géodynamique, UFR des Sciences et des Techniques, Université de Nantes, France*

Received 3 June 2005; received in revised form 14 October 2005; accepted 20 October 2005

Abstract

Most techniques used in seismological practice have been performed under the assumption that surface waves propagate along great circle arcs between the epicenter and the station. However, lateral variations of surface wave phase velocities should result in deviation of the wave paths from great circle arcs and in corresponding anomalies of geometrical spreading (so-called focusing effect). We performed numerical modeling of these effects using the ray approximation on the basis of recent global phase velocity maps for fundamental Rayleigh mode obtained by tomographic inversion in the period range from 60 to 150 s.

The aim for such a modeling is to investigate where the conventional methods based on using great circles as paths fail, and to obtain quantitative characteristics for the effects of rays focusing.

Predicted and observed focusing effects are analyzed from a statistical point of view on a dataset of real seismic data. Records of earthquakes in a wide magnitude range ($6 < M_s < 7$) and with epicenters in different seismic regions are used for the analysis (over 3000 measurements). Synthetic and observed Rayleigh wave amplitude spectra are found to be in better agreement when the focusing effect is taken into account: correction of spectra for predicted focusing effect significantly improves the fit of synthetics to observations at periods larger than 75 s.

Calculation of focusing effect based on ray theory ignores the effects of wavefront smoothing which increases with increasing period. However, even this approximation gives considerable improvement of synthetics at periods up to 150 s and, therefore, can be used in many applications, such as seismic source studies, magnitude measurements, and Q estimates.

We also demonstrated that the discrepancy between real data and synthetics cannot be explained by attenuation effects. It means that there is still large room for improvement of the existing tomographic models which, in order to correctly explain observed amplitudes, must include heterogeneity of anisotropy and anelasticity up to higher degree.

© 2006 Elsevier B.V. All rights reserved.

Keywords: Ray theory; Surface waves; Lateral heterogeneities; Focusing effect; Attenuation

1. Introduction

Surface waves recorded at teleseismic distances contain information both on the earthquake source parameters and on the Earth's structure along the source-station

* Corresponding author. Tel.: +33 14427 4895; fax: +33 14427 3894.
E-mail address: jpm@ipgp.jussieu.fr (J.-P. Montagner).

path. These waves convey most of the long period energy (periods longer than 20 s) and are characterized by a high signal-to-noise ratio. This is the reason why surface waves are widely used in seismology for studying the crust and upper mantle structure and seismic source parameters.

Most techniques used in seismological practice are based on the assumption that surface waves propagate along great circle paths. At the same time the results of tomographic studies show that the amplitude of lateral variations of surface wave phase velocities can be as large as 10%. Such variations should result in deviations of the wave paths from great circles and consequent anomalies of surface wave amplitudes and polarization (see Romanowicz, 2002 for a review). In particular the amplitude and phase anomalies should be associated with focusing and defocusing effects related to caustics formed by intersection of surface wave paths at large epicentral distances, strongly pronounced for multi-orbit waves, e.g. R2, R3, etc.

This effect was noted by Lay and Kanamori (1985) and Jobert and Jobert (1987) when modeling long period surface wave paths. Woodhouse and Wong (1986) and Wang and Dahlen (1994) studied the amplitude and phase anomalies in slowly varying laterally heterogeneous media using the first order ray perturbation theory. Wang and Dahlen (1994) developed a numerically efficient implementation of the JWKB approximation to derive the same anomalies and then compared the results with the corresponding ones obtained by using the first order ray perturbation theory. Wang et al. (1993) and Dahlen and Tromp (1998) presented the results of a calculation of the R2–R3 and R1–R2 wave paths in the vicinity of an epicenter and its antipode. They demonstrate that the intersection of the rays forms many caustics. The caustics have a specific shape: they consist of two branches, which form cusps in the points of their merging. Yanovskaya (2004) has shown that the wave amplitudes in the vicinity of such a caustic are described by the Pearcey integral (Pearcey, 1946), and that the amplitudes differ substantially from those calculated on the basis of the ray theory. Wang and Dahlen (1995) considering the Fresnel area along the surface wave ray path obtained the necessary and sufficient condition for the validity of the JWKB approximation in laterally heterogeneous media. They have shown that the misfit of the ray approximation related to this condition can be attributed to the wavefront smoothing produced by the Fresnel area along the ray path. This finite frequency effect is ignored in the ray theory, and, therefore, the JWKB estimates of the focusing effect tend to be overestimated when the scale length of lateral heterogeneity is close to the wave-

length of the surface waves. A number of studies were dedicated to investigation of the limitations of ray theory, as well as to generalization of the methods of surface wave studies incorporating the effects of finite frequency (e.g., Hung et al., 2001; Spetzler et al., 2002; Yoshizawa and Kennett, 2002, 2004; Tanimoto, 2003; Zhou et al., 2004).

Recently, more sophisticated techniques for simulation of wave propagation in heterogeneous media, such as a method based on spectral elements (Komatitsch et al., 2002) also demonstrated large deviation of the observed amplitude compared with synthetic amplitude.

However, if the lateral scale of heterogeneity is much larger than the wavelength of surface waves, then it is possible to use efficiently the ray theory for calculation of surface wave amplitudes outside the caustics. In this paper we calculate the surface wave amplitude anomalies in the JWKB approximation. The applicability of this approach is discussed in Section 4. On the basis of ray theory, surface wave ray paths are calculated and geometrical spreading for a given map of phase velocity anomalies and a given location of the epicenter is estimated. The amplitude anomaly is defined as the ratio of the calculated amplitude in the laterally heterogeneous sphere to that in a spherically symmetric model. Below we name the effect of the geometrical spreading anomalies on the amplitudes as *focusing effect*, though the rays can converge (focusing) or diverge (defocusing). The amplitude anomalies are calculated on a grid on the Earth's surface. We calculated the spectral amplitude anomalies for Rayleigh waves within the period range 60–150 s using recent global isotropic phase velocity maps (Beucler, 2002; Beucler and Montagner, in press).

Additional cause for the amplitude anomalies is anelastic attenuation, which can be different on different paths due to lateral variation of anelasticity. We compare these two effects: the focusing effect due to geometrical spreading and the effect of lateral variation of anelasticity.

It is practically useless to look for focusing effect by direct comparison of calculated and observed surface wave amplitudes on individual records, because the maps of lateral velocity variations are rather smoothed and do not include all peculiarities of the velocity pattern. Another cause of a possible discrepancy between calculated and observed amplitudes is the uncertainty in the determination of the source model that may affect strongly the calculated amplitudes. Therefore it is worthwhile to compare the calculated and observed amplitudes statistically, on a large data set of seismograms corresponding to different events and stations. Such a comparison was performed by using records of earth-

quakes with $6 < M_s < 7$ occurring in different seismic regions. The decrease of misfit between synthetic and observed Rayleigh wave amplitude spectra when allowing the focusing effect confirms the possibility to take into account the ray approximation estimates of surface wave amplitude anomalies in routine seismological studies based on dynamic characteristics of surface waves.

2. Surface wave spectra

We approximate the elastic model of the Earth by a weak laterally inhomogeneous model (Woodhouse, 1974; Babich et al., 1976). The spectrum of displacements $\mathbf{u}(\omega)$ in surface wave generated by an instant point source in such a model (Levshin et al., 1989) can be expressed in form

$$\mathbf{u}(\mathbf{x}_r, \omega) = \frac{\exp(-i\pi/4) \exp(-i\omega\tau)}{\sqrt{8\pi} \sqrt{\omega J/c}} \times \frac{\chi(\mathbf{x}_s, \gamma, \omega) \mathbf{U}(\mathbf{x}_r, \omega)}{\sqrt{cvI|_s} \sqrt{cvI|_r}} q(\mathbf{x}_r, \omega). \quad (1)$$

where ω is the angular frequency, \mathbf{x}_s and \mathbf{x}_r the coordinates of the source and of the registration point, γ the ray azimuth in the source, c and v the phase and group velocity of the wave, χ the radiation pattern of the source dependent on the moment tensor, eigenfunctions and their derivatives in the source vicinity, and direction of radiation, \mathbf{U} the eigenfunction describing the distribution of displacements in the wave along the vertical direction, q a factor describing the wave attenuation, I the energy integral of eigenfunction, s and r are, respectively, the indices of the source and receiver, J the geometrical spreading, and τ is the wave arrival time. So, the surface wave spectrum in this approximation is determined by the near source and near receiver velocity structure, by the average phase velocity and attenuation along the wave path, and by geometrical spreading. At the same time the amplitude spectrum does not depend on the average phase velocity of the wave. In such a model the errors in source location do not affect the amplitude spectrum (Bukchin, 1990). For spherical symmetric Earth model we have $\tau = R\Delta/c_0$, $q = \exp[-\omega Q_0^{-1} R\Delta/(2c_0)]$, $J = R \sin \Delta$. Here R is the Earth radius, Δ is the epicentral distance, c_0 is the value of phase velocity of the wave, and Q_0 is the surface wave quality factor. In the case of a weakly laterally inhomogeneous medium we are able to calculate the arrival time, attenuation and geometrical spreading of the wave integrating the systems of equations for kinematic and dynamic ray tracing.

3. Equations for kinematic and dynamic ray tracing

The system of equations for kinematic ray tracing on a sphere is obtained from the general equations for ray. It has the form (Julian, 1970; Aki and Richards, 1980):

$$\begin{aligned} \frac{d\theta}{d\tau} &= -\frac{c(\theta, \varphi) \cos \alpha}{R} & \frac{d\varphi}{d\tau} &= c(\theta, \varphi) \frac{\sin \alpha}{R \sin \theta} \\ \frac{d\alpha}{d\tau} &= -\frac{1}{R} \left(\sin \alpha \frac{\partial c}{\partial \theta} + \frac{\cos \alpha}{\sin \theta} \frac{\partial c}{\partial \varphi} \right) + \frac{c \sin \alpha}{R \tan \theta}. \end{aligned} \quad (2)$$

where θ , φ are spherical coordinates, R radius of the sphere, α the ray azimuth at the current point, c the phase velocity, and τ is the propagation time. The coordinates of a source θ_0 , φ_0 and azimuth of the ray in the source α_0 are the initial conditions (at $\tau=0$) for integration of this system.

To construct the system for dynamic ray tracing we apply the usual approach: by considering the new functions

$$\frac{\partial \theta}{\partial \gamma} = S_1, \quad \frac{\partial \varphi}{\partial \gamma} = S_2 \quad \text{and} \quad \frac{\partial \alpha}{\partial \gamma} = P,$$

where γ is the ray azimuth in the source, and differentiate Eq. (2) with respect to γ . Then the equations for S_1 , S_2 and P are found to be as follows:

$$\begin{aligned} \frac{dS_1}{d\tau} &= \frac{Pc \sin \alpha}{R} - \left(\frac{\partial c}{\partial \theta} S_1 + \frac{\partial c}{\partial \varphi} S_2 \right) \frac{\cos \alpha}{R} \\ \frac{dS_2}{d\tau} &= \frac{Pc \cos \alpha}{R \sin \theta} - \frac{S_1 c \cos \theta \sin \alpha}{R \sin^2 \theta} \\ &\quad + \left(\frac{\partial c}{\partial \theta} S_1 + \frac{\partial c}{\partial \varphi} S_2 \right) \frac{\sin \alpha}{R \sin \theta} \\ \frac{dP}{d\tau} &= \frac{P}{R} \left(-\frac{\partial c}{\partial \theta} \cos \alpha + \frac{\sin \alpha}{\sin \theta} \frac{\partial c}{\partial \varphi} + c \frac{\cos \alpha}{\tan \theta} \right) \\ &\quad + \frac{S_1}{R \sin^2 \theta} \left(\cos \alpha \cos \theta \frac{\partial c}{\partial \varphi} - c \sin \alpha \right) \\ &\quad + \left(\frac{\partial c}{\partial \theta} S_1 + \frac{\partial c}{\partial \varphi} S_2 \right) \frac{\sin \alpha}{R \tan \theta} \\ &\quad - \left(\frac{\partial^2 c}{\partial \theta^2} S_1 + \frac{\partial^2 c}{\partial \theta \partial \varphi} S_2 \right) \frac{\sin \alpha}{R} \\ &\quad - \left(\frac{\partial^2 c}{\partial \theta \partial \varphi} S_1 + \frac{\partial^2 c}{\partial \varphi^2} S_2 \right) \frac{\cos \alpha}{R \sin \theta}. \end{aligned} \quad (3)$$

Initial conditions for integration of this system are the following:

$$S_1 = S_2 = 0, \quad P = 1.$$

The functions S_1 and S_2 obtained from the system of Eq. (3) determine the geometrical spreading:

$$J = R(S_1 \sin \alpha + S_2 \cos \alpha \sin \theta). \quad (4)$$

To calculate the attenuation factor it is necessary to add the equation

$$\frac{d\psi}{d\tau} = \frac{1}{Q(\theta, \varphi)}, \quad (5)$$

where $Q(\theta, \varphi)$ is the surface wave quality factor, with the initial condition $\psi(0)=0$. Then the attenuation factor $q = \exp(-(\omega\psi/2))$. Eqs. (2), (3) and (5) should be integrated jointly.

To calculate the values of the geometrical spreading and the attenuation factor at a given receiver point (station) from a given source point (epicenter) we used the shooting method.

4. Numerical modeling of wave field anomalies

We perform numerical modeling of the effects due to a weak and smooth lateral inhomogeneity of the elastic Earth model using global phase velocity anomaly maps for fundamental Rayleigh mode in the period range from 60 to 150 s (Beucler, 2002; Beucler and Montagner, in press). The distribution of velocity anomalies and errors of their determination on the Earth surface are given by spherical harmonics expansion up to degree 20. Examples of such maps for period of 75 s are given in Fig. 1. The maps are plotted in azimuthal equidistant projection for two hemispheres. Both velocity anomalies and errors are measured in percentage with respect to the reference velocity value for spherically symmetric model PREM (Dziewonski and Anderson, 1981).

For a given location of the epicenter we calculate the propagation time τ , attenuation factor q and geometrical spreading J by integrating the systems (2), (3) and Eq. (5). We calculate these quantities in different points of

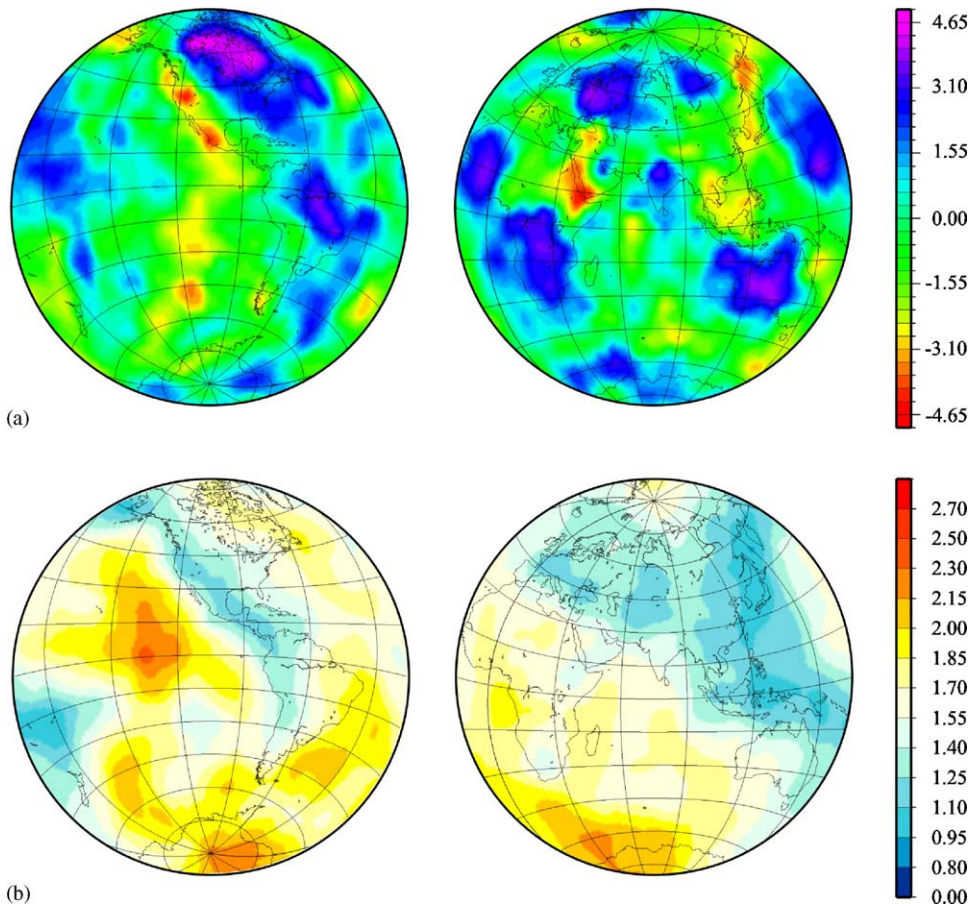


Fig. 1. (a) Phase velocity anomalies (%) and (b) errors (%) of phase velocity anomalies determination for fundamental Rayleigh mode at period 75 s.

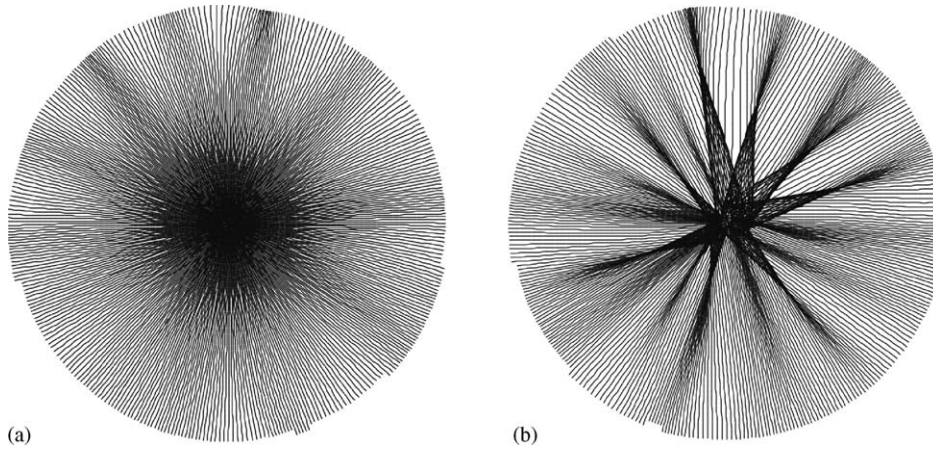


Fig. 2. Scheme of rays for 75 s Rayleigh fundamental mode (a) for the hemisphere centered at the epicenter and (b) for the hemisphere centered at the epicenter’s antipode. The epicenter is located in Indonesia ($-1^\circ, 124^\circ$).

rays radiated in the whole range of azimuths in order to get a map of the amplitude anomalies for a given source, as well as in a given location of stations.

An example of a scheme of rays for fundamental Rayleigh mode for period 75 s is presented in Fig. 2. The epicenter is located in Indonesia. The rays are drawn in azimuthal equidistant projection. The rays deviate negligibly from the great circle arcs at distances less than 90° , but in the opposite hemisphere ($90^\circ < \Delta < 180^\circ$) the deviations become significant.

As can be seen from Fig. 2, a multipathing area bounded by caustics appears in a really wide area around the epicenter antipode. Geometrical spreading is vanishing at a caustic and becomes negative behind the point of contact. Numerical calculations show that among the rays passing any point of the multipathing area there exists at least one ray tangent to the caustic. These fea-

tures of the ray field are caused by two factors: lateral heterogeneity of the Earth and spherical geometry.

We define the amplitude anomaly due to deviation of the ray from the great circle arc by calculating the focusing coefficient f that is the ratio of spectral amplitudes in the laterally inhomogeneous Earth model and in the spherically symmetric model. As follows from formula (1), the value of f can be calculated by formula $f = \sqrt{R \sin \Delta / J}$, where the geometrical spreading J is determined from (4) after integrating (2), (3).

The amplitude anomaly map (the spatial distribution of focusing coefficient f) corresponding to the scheme of rays for the fundamental Rayleigh mode for period 75 s is presented in Fig. 3. The map is plotted in azimuthal equidistant projection for two hemispheres centered at the epicenter and at the epicenter antipode. The amplitude anomalies are calculated on the rays covering the

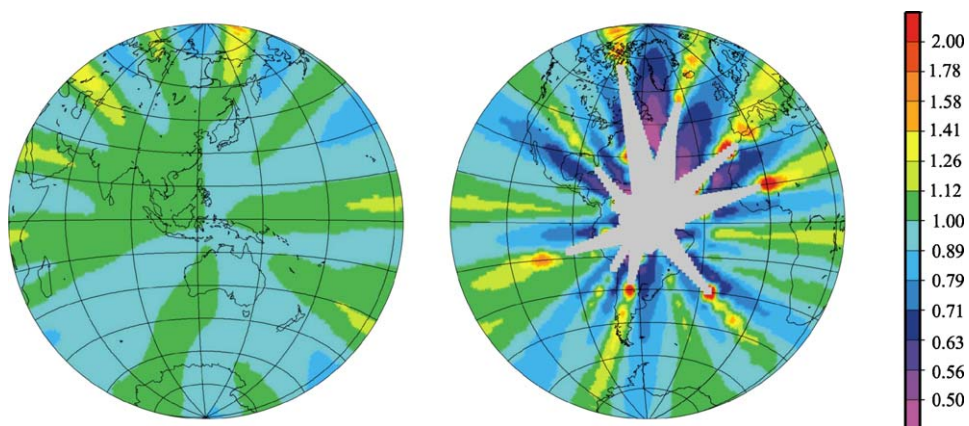


Fig. 3. Map for amplitude anomalies for 75 s Rayleigh fundamental mode. The epicenter is located in Indonesia ($-1^\circ, 124^\circ$). Multipathing area is shaded gray.

entire Earth surface except the shaded gray area corresponding to multipathing. As seen from Fig. 3, strong anomalies appear at epicentral distances $\Delta > 90^\circ$. But they can be significant at shorter distances as well.

Wang and Dahlen (1995) have shown that amplitude anomalies obtained using the JWKB approximation can be overestimated when the scale length of lateral heterogeneity is insufficiently large in comparison to the wavelength of the surface waves. On the other hand excessive smoothing makes the model nonrealistic. Wang and Dahlen (1995) considering contrived degree-36 model as ‘ground truth’ model of the Earth compared the errors due to the JWKB approximation with errors due to truncation in the model for 150 s fundamental Rayleigh mode. They have found for this model that the total amplitude misfit due to the two error sources attained its minimum value at about degree 17. Taking into account the complexity of the real Earth we use degree-20 model for calculation of the synthetic amplitude spectra and compare the results with real observations. At the same time to avoid the overestimated amplitude anomalies due to the limitations of the ray theory we consider paths with focusing coefficients in the range $0.5 < f < 1.5$.

5. Effects of lateral variations of anelasticity on surface wave amplitude spectra

Lateral variations of anelasticity also cause deviations of surface wave amplitude spectra from those expected in spherically symmetric Earth. We measure corresponding amplitude anomaly by a ratio of q factors calculated for a Q model for laterally inhomogeneous Earth and for constant Q .

The amplitude anomalies due to lateral variations of anelasticity are compared with those caused by focusing effect for fundamental Rayleigh mode at the period of 150 s. The global map of local attenuation (Romanowicz, 1995) is calculated from the expansion of Q in spherical harmonics up to degree 10. The lateral resolution of this map is significantly different from those of degree-20 model for phase velocity anomalies. But it is more correct to compare these two effects using models with similar order of lateral heterogeneities. For this reason, we calculate amplitude anomalies caused by focusing effect, when using smoothed model for phase velocity anomalies truncated up to degree-10.

We selected 25 seismofocal zones from all over the world (Fig. 4). For each epicenter zone attenuation effect and focusing effect are calculated for 252 stations of the worldwide FDSN seismic network, representing a total amount of 6187 paths except 113 paths intersect-

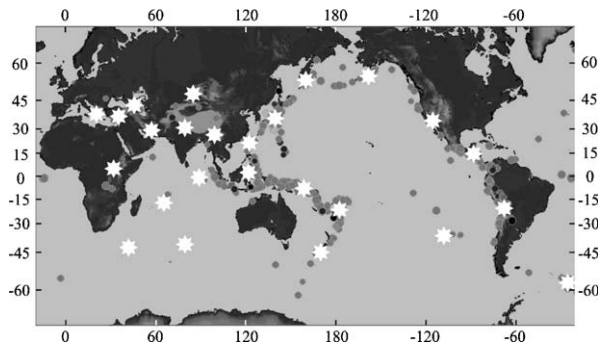


Fig. 4. World seismicity ($6.5 < M_s < 7.0$) for period from 1990 to 2000 and focal zones (stars) selected for the study of effects related to the deviation from spherical symmetry of the elastic and anelastic Earth models.

ing multipathing areas or related to stations located in the vicinity of epicenter. The results of comparison of the focusing effect and the effect of lateral variations of anelasticity are shown in 2D diagram for relative q factor and focusing coefficient in Fig. 5. Every circle at the diagram corresponds to one path. As can be seen from Fig. 5, there is no correlation between focusing effect and q factor effect and the focusing effect caused by lateral inhomogeneity of the elastic Earth model can be significantly larger than the effect related to the lateral inhomogeneity of attenuation for fundamental Rayleigh mode at the period of 150 s. In further analysis we assumed Q values for spherically symmetric model PREM.

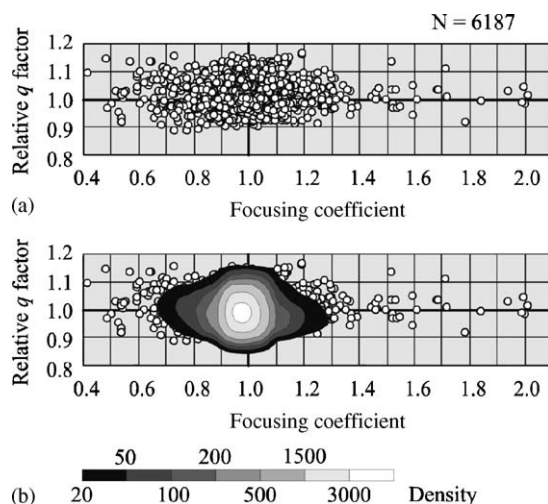


Fig. 5. (a) Comparison of amplitude anomalies caused by focusing effect and by asphericity of attenuation model for Rayleigh fundamental mode ($T = 150$ s). Every circle corresponds to one of paths. (b) The same diagram as (a), superimposed by a map for circles density (number of circles in a square 0.1×0.1).

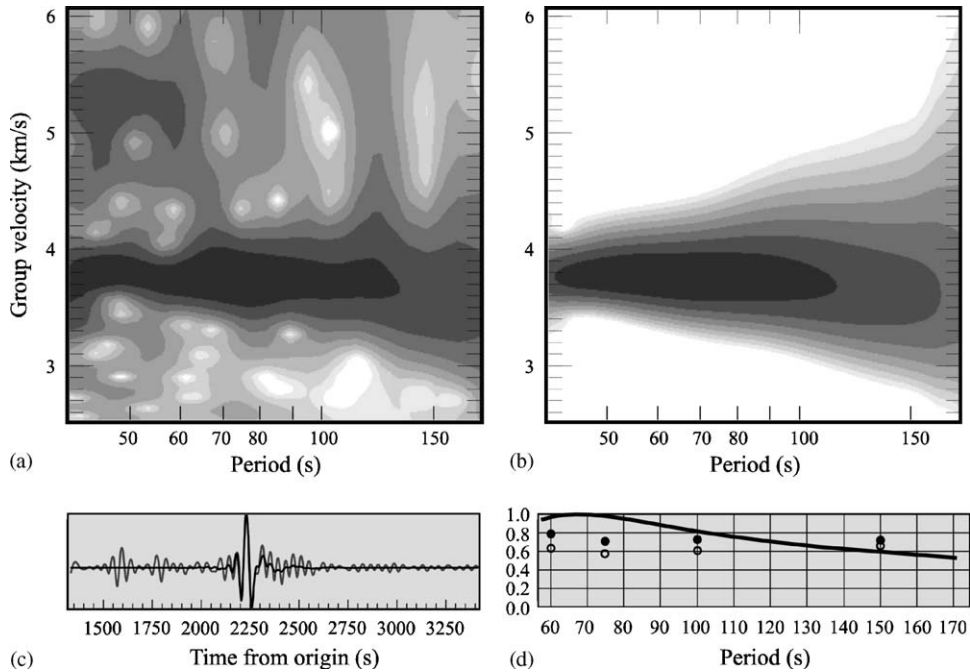


Fig. 6. Example of frequency–time analysis (FTAN) and floating filtering for Kamchatka earthquake record at IRIS/USGS station HKT in Hockley, Texas, isolating fundamental Rayleigh mode and comparison of amplitude spectrum of filtered wave with synthetic values. FTAN diagrams for (a) raw and (b) floating-filtered vertical component. (c) Vertical component of raw record (gray line) and floating-filtered (black line), normalized to maximum value. (d) Amplitude spectrum of floating-filtered record (solid line) and two synthetic values: with (filled circles) and without the focusing effect (open circles). The spectra are normalized to their maximum value.

6. Comparison of predicted focusing effect with observations

We perform the comparison of predicted and observed amplitude anomalies in fundamental Rayleigh wave by using broadband records of 106 earthquakes ($6 < M_s < 7$) located in the 25 seismic zones presented in Fig. 4. Using frequency–time analysis technique and floating filtering (Levshin et al., 1989) we isolate fundamental Rayleigh mode for about 1400 paths. We reject signals recorded within the multipathing area or at distances from caustics less than one and a half wavelength. We use records of a good quality in period range from 60 to 150 s. We calculate amplitude spectrum for the periods of 60, 75, 100 and 150 s for all filtered records. The spectra are corrected for the instrument response. Synthetic spectra are calculated by formula (1) with the use of the CMT solutions for normalized moment tensor from Harvard catalog and seismic moments, which are recalculated on the basis of the seismic records. The structure models in the source and under the station are taken from the 3SMAC model (Ricard et al., 1996). For every observed value of the amplitude spectra we calculate two synthetic values: with and without the focusing effect. To calculate the focusing effect f , Eqs. (2) and (3) are integrated and

the shooting method is used to obtain the result in a given station location. Simultaneously with the focusing effect, the average errors β of the velocity anomaly along the rays that characterize the reliability of f estimate, are calculated.

An example of frequency–time analysis and floating filtering for Kamchatka earthquake, 25.06.1996 ($M_s = 6.6$) record at IRIS/USGS station HKT in Hockley, Texas, isolating fundamental Rayleigh mode is given in Fig. 6(a)–(c). The epicentral distance for HKT station is about 75° . The wave propagates along the regions with dense path coverage for tomographic models and for all the four periods under consideration the path belong to 25% of best paths with least average error β . The focusing coefficient f takes values 1.251, 1.237, 1.184 and 1.093 for respective periods of 60, 75, 100 and 150 s. The amplitude spectrum of isolated fundamental Rayleigh mode and two synthetic values (without taking into account the focusing effect and taking it into account) are shown in Fig. 6(d).

6.1. Data sampling

The total number of selected measurements is equal to 3256. We consider different samples of observations

and corresponding synthetics according to the value of the focusing coefficient f and the value of average error β . Along with samples containing paths characterized by any value of f varying from 0.5 to 1.5 we consider corresponding samples containing paths characterized by strong focusing effect ($f > 1.25$ or $f < 0.75$). The total number of measurements corresponding to paths with strong focusing effect is equal to 786. The distribution of the number of measurements versus period is given in Table 1.

Using value of average error β for characterization of the reliability of f estimate we consider samples corresponding to different quantiles of best paths.

6.2. Characterization of misfit

Let ε_{qi} and ε_{qcorr} be the misfit between synthetic and observed amplitude spectra for i -th measurement of q -th earthquake calculated, respectively, without taking into account the focusing effect and taking it into account. Let N_q be the number of such measurements, m_{0q} - the seismic moment of the q -th earthquake. We characterize the misfit for q -th earthquake by rms values of ε_{qi} and ε_{qcorr} normalized by seismic moment:

$$E_q = \frac{1}{m_{0q}} \sqrt{\frac{\sum_{i=1}^{N_q} \varepsilon_{qi}^2}{N_q}}, \quad E_{qcorr} = \frac{1}{m_{0q}} \sqrt{\frac{\sum_{i=1}^{N_q} \varepsilon_{qcorr}^2}{N_q}}.$$

We define the average reduction of absolute misfit as difference between these two values averaged over all earthquakes:

$$\Delta \langle E \rangle = \langle E \rangle - \langle E_{corr} \rangle.$$

The ratio $\Delta \langle E \rangle / \langle E \rangle$ in percentage for the total of four considered periods and for each period separately is shown in Fig. 7. The ratio characterizing the reduction of misfit is given for four different samples corresponding to different quantiles of best paths with least average error β (best 25% of paths, best 50%, best 75%, and 100% corresponds to the total sample).

We present separately the results for samples corresponding to the entire range of focusing effect ($0.5 \leq f \leq 1.5$) and the results for paths with strong focusing effect ($f \leq 0.75$ or $1.25 \leq f$).

Table 1
Distribution of the number of measurements vs. period

| f value/period (s) | 60 | 75 | 100 | 150 |
|--------------------------------|-----|-----|-----|-----|
| $0.5 \leq f \leq 1.5$ | 802 | 895 | 872 | 687 |
| $f \leq 0.75$ or $1.25 \leq f$ | 263 | 276 | 167 | 80 |

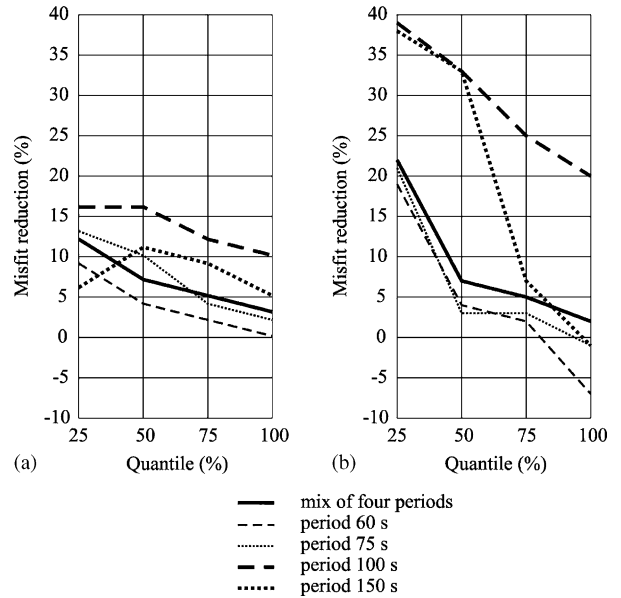


Fig. 7. Reduction of misfit for different periods. (a) Entire range of focusing effect and (b) strong focusing effect.

7. Discussion of the results

If the estimates of focusing effects are valid in general, one should expect larger reduction of misfit caused when taking into account these effects for traces with smaller averaged error of tomographic maps β . The results presented in Fig. 7 confirm such an expectation. As one can see from Fig. 1(b) the errors are small in particular regions with good path coverage for tomographic models, such as in the northern hemisphere and the Pacific rim, while the errors become larger in the southern hemisphere and oceanic regions. For samples including all paths (100% quantiles) the reduction of misfit is vanishing or becomes even negative, which means an increase of misfit. The improvement of fitting becomes considerable for paths characterized by small error β and strong focusing effect. Usually rays deviate negligibly from the great circle arcs at distances less than 90° . As a rule for such distances the conventional ray theoretical methods with the approximation of the great circle paths may work well. However, as could be seen from Fig. 3, this deviation and related anomalies can be significant even at shorter distances.

The results obtained for different periods visibly differ from each other. The most significant improvement is achieved for periods 100 and 150 s. The misfit estimates depend on velocity anomaly maps as well as on the maps for errors of velocity anomalies determination. So, the difference of results for different

periods may reflect the different quality of both kinds of maps.

The results confirm that phase velocity maps are the best resolved at periods longer than 75 s. At the period of 100 s the ray theory is valid, and the improvement of synthetics is significant for most of the traces. At the 150 s period the ray approximation is still valid, at least in the regions where the error of tomographic map is small. At periods shorter than 100 s the amplitudes of heterogeneities is much stronger and effects such as scattering due to anisotropy and small scale scatterers can have large influence on amplitude. Other tomographic models (Montagner, 2002; Ekström et al., 1997) were tested, but are not presented here since the conclusions are not affected by the choice of these other tomographic models.

So, there is still a large room for improvement of tomographic models below periods of 100 s, by including effects of anelasticity, anisotropy and small scatterers. However, for long periods, it seems important to correct the surface wave spectra for focusing effect in order to avoid biases in the determinations of seismic moments and focal mechanisms.

8. Conclusions

Presented results of numerical modeling and analysis of real seismic records show that synthetic and observed Rayleigh wave amplitude spectra are in better agreement when the focusing effect is taken into account. The improvement of the fit of synthetics to observations is sensitive to the averaged accuracy of tomography maps along ray path. It is substantially large for paths with high average accuracy and strong focusing effect exceeding the errors due to other factors, such as lateral inhomogeneity of attenuation, errors of source parameters determination, scattering effects, etc.

Ray theory used in this study for focusing effect calculation ignores finite frequency effects. But even this approximation gives considerable improvement of synthetics based on great-circle path approximation at periods up to 150 s and can be used in many applications: seismic source study, magnitude measurements, and Q estimation.

Ray theory is inapplicable in the vicinities of caustics and in multipathing areas. It can be used only for rough estimates of multipathing area boundaries. For calculations of surface waves near the caustics and inside the multipathing areas more sophisticated techniques such as coupled-mode or spectral-element methods should be used.

Acknowledgments

This research was done while BB and AM were visiting the Institut de Physique du Globe de Paris, thanks to a grant from MESR in France. BB and AM are also supported by Basic Research Program 13 “Changes of Environment and Climate: Natural Disasters” of the Presidium of Russian Academy of Sciences. TY was supported by Russian Foundation of Basic Research grant RFBR 05-05-64164. The authors would like to acknowledge the GEOSCOPE datacenter and IRIS-DMC for providing data used in this paper. The paper benefited of discussions with A. Lander and E. Clevede. Reviews by anonymous reviewers helped considerably to clarify and improve the manuscript.

References

- Babich, V.M., Chikachev, B.A., Yanovskaya, T.B., 1976. Surface waves in a vertically inhomogeneous elastic half-space with weak horizontal inhomogeneity. *Izv. Akad. Nauk SSSR Fizika Zemli* 4, 24–31.
- Beucler, E., 2002. Regional and global tomography of the Earth mantle: approach from body and surface waves. Ph.D. Thesis. Institut de Physique du Globe de Paris.
- Beucler, E., Montagner, J.-P., in press. Computation of large anisotropic seismic heterogeneities (CLASH). *Geophys. J. Int.*
- Bukchin, B.G., 1990. Determination of source parameters from surface waves recordings allowing for uncertainties in the properties of the medium. *Izv. Akad. Nauk SSSR Fizika Zemli* 25, 723–728.
- Dahlen, F.A., Tromp, J., 1998. *Theoretical Global Seismology*. Princeton University Press, p. 1025.
- Dziewonski, A.M., Anderson, D.L., 1981. Preliminary reference earth model. *Phys. Earth Planet. Int.* 25, 297–356.
- Ekström, G., Tromp, J., Larson, E.W., 1997. Measurements and global models of surface wave propagation. *J. Geophys. Res.* 102, 8137–8157.
- Hung, S.-H., Dahlen, F., Nolet, G., 2001. Wavefront healing: a banana–doughnut perspective. *Geophys. J. Int.* 146, 289–312.
- Jobert, N., Jobert, G., 1987. Ray tracing for surface waves. In: Nolet, G. (Ed.), *Seismic Tomography*. Reidel, Dordrecht, pp. 275–300.
- Julian, B.R., 1970. Ray tracing in arbitrarily heterogeneous media. Technical Note. 1970-45. Lincoln Laboratory, Mass. Institute of Technology, Cambridge.
- Lay, T., Kanamori, H., 1985. Geometrical effects of global lateral heterogeneity on long-period surface wave propagation. *J. Geophys. Res.* 90 (B1), 605–621.
- Levshin, A.L., Yanovskaya, T.B., Lander, A.V., Bukchin, B.G., Barmine, M.P., Ratnikova, L.I., Its, E.N., 1989. In: Keilis-Borok, V.I. (Ed.), *Seismic Surface Waves in a Laterally Inhomogeneous Earth*. Kluwer Academic Publishers, Dordrecht, p. 293.
- Komatitsch, D., Ritsema, J., Tromp, J., 2002. The spectral-element method, Beowulf computing, and three-dimensional seismology. *Science* 298, 1737–1742.
- Montagner, J.-P., 2002. Upper mantle low anisotropy channels below the Pacific Plate. *Earth Planet. Sci. Lett.* 202, 263–274.
- Pearcey, T., 1946. The structure of an electromagnetic field in the neighborhood of a cusp of a caustic. *Philos. Mag.* 37, 311–317.

- Ricard, Y., Nataf, H.-C., Montagner, J.-P., 1996. The three-dimensional seismological model a priori constrained: confrontation with seismic data. *J. Geophys. Res.* 101, 8457–8472.
- Romanowicz, B., 1995. A global tomographic model of shear attenuation in the upper mantle. *J. Geophys. Res.* 100 (B7), 12375–12394.
- Romanowicz, B., 2002. Inversion of surface waves: a review. In: Lee, W.H.K., Kanamori, H., Jennings, P.C., Kisslinger, C. (Eds.), *International Handbook of Earthquake and Engineering Seismology, Part A*. Academic Press, San Diego, pp. 149–173.
- Spetzler, J., Trampert, J., Snieder, R., 2002. The effect of scattering in surface wave tomography. *Geophys. J. Int.* 149, 755–767.
- Tanimoto, T., 2003. Geometrical approach to surface wave finite frequency effects. *Geophys. Res. Lett.* 30 (19), 1993, doi:10.1029/2003GL017475.
- Wang, Z., Dahlen, F.A., 1994. JWKB surface-wave seismograms on a laterally heterogeneous Earth. *Geophys. J. Int.* 119, 381–401.
- Wang, Z., Dahlen, F.A., 1995. Validity of surface-wave ray theory on a laterally heterogeneous Earth. *Geophys. J. Int.* 123, 757–773.
- Wang, Z., Dahlen, F.A., Tromp, J., 1993. Surface-wave caustics. *Geophys. J. Int.* 114, 311–324.
- Woodhouse, J.H., 1974. Surface waves in the laterally varying structure. *Geophys. J. R. Astr. Soc.* 90, 713–728.
- Woodhouse, J.H., Wong, Y.K., 1986. Amplitude, phase and path anomalies of mantle waves. *Geophys. J. R. Astr. Soc.* 87, 753–773.
- Yanovskaya, T.B., 2004. Peculiarities of surface wave field in the vicinity of caustics contact. *Phys. Solid Earth* 40 (12), 965–972.
- Yoshizawa, K., Kennett, B.L.N., 2002. Determination of the influence zone for surface wave paths. *Geophys. J. Int.* 149, 440–453.
- Yoshizawa, K., Kennett, B.L.N., 2004. Multi-mode surface wave tomography for the Australian region using a three-stage approach incorporating finite frequency effects. *J. Geophys. Res.* 109, B02310, doi:10.1029/2002JB002254.
- Zhou, Y., Dahlen, F.A., Nolet, G., 2004. Three-dimensional sensitivity kernels for surface wave observables. *Geophys. J. Int.* 158, 142–168.